Faraday Discussions

Cite this: *Faraday Discuss.*, 2018, **206**, 219



PAPER

# Structure and lifetimes in ionic liquids and their mixtures†

Sascha Gehrke, [ab] Michael von Domaros,[a] Ryan Clark,[d] Oldamur Hollóczki, [a] Martin Brehm, [c] Tom Welton, [d] Alenka Luzar[e] and Barbara Kirchner *[a]

Received 9th May 2017, Accepted 10th July 2017
DOI: 10.1039/c7fd00166e

With the aid of molecular dynamics simulations, we study the structure and dynamics of different ionic liquid systems, with focus on hydrogen bond, ion pair and ion cage formation. To do so, we report radial distribution functions, their number integrals, and various time–correlation functions, from which we extract well-defined lifetimes by means of the reactive flux formalism. We explore the influence of polarizable force fields *vs.* non-polarizable ones with downscaled charges (±0.8) for the example of 1-butyl-3-methylimidazolium bromide. Furthermore, we use 1-butyl-3-methylimidazolium trifluoromethanesulfonate to investigate the impact of temperature and mixing with water as well as with the chloride ionic liquid. Smaller coordination numbers, larger distances, and tremendously accelerated dynamics are observed when the polarizable force field is applied. The same trends are found with increasing temperature. Adding water decreases the ion–ion coordination numbers whereas the water–ion and water–water coordination is enhanced. A domain analysis reveals that the nonpolar parts of the ions are dispersed and when more water is added the water clusters increase in size. The dynamics accelerate in general upon addition of water. In the ionic liquid mixture, the coordination number around the cation changes between the two anions, but the number integrals of the cation around the anions remain constant and the dynamics slow down with increasing content of the chloride ionic liquid.

[a]*Mulliken Center for Theoretical Chemistry, University of Bonn, Beringstr. 4+6, D-53115 Bonn, Germany. E-mail: kirchner@thch.uni-bonn.de*

[b]*Max Planck Institute for Chemical Energy Conversion, Stiftstr. 34-36, D-45413 Mülheim an der Ruhr, Germany*

[c]*Theoretical Chemistry, Martin-Luther-University Halle-Wittenberg, Universitätsplatz 10, D-06108 Halle, Germany*

[d]*Imperial College London, South Kensington Campus, London SW7 2AZ, UK*

[e]*Department of Chemistry, Virginia Commonwealth University, Richmond, Virginia 23284-2006, USA*

† Electronic supplementary information (ESI) available. See DOI: 10.1039/c7fd00166e

# 1 Introduction

Many properties of ionic liquids (ILs),[1] with much emphasis on their structures[2–6] and some references to slow dynamics (for an overview, see ref. 7), have been widely discussed by theoretical methods in the literature.[2,3,5,6] For example, the mesoscopic segregation[8] of the polar and nonpolar moieties in the liquid has been studied by theory qualitatively[9–11] and quantitatively.[5,12–15] However, their hydrogen bond (how long does a hydrogen bond (HB) exist?) and ion pair (how long does an ion pair (IP) exist?) as well as ion cage (IC) (how long is an ion surrounded by the counter-ions?) fast dynamics have not been this intensively considered.[16–22]

Most hydrogen bonds are non-linear in ILs, especially if the ILs are apolar and based on imidazolium cations, such that the donor is a C–H group[23] which is well-known in the literature to form weak hydrogen bonds.[24,25] This particular non-linearity was explained by Hunt and coworkers[26,27] as a stabilisation by areas of local electron depletion, which occurs between the substituents on the imidazolium ring. The regions of reduced electron density extend over quite a large area, thus allowing anions to adjust relatively freely instead of strictly being linear.[26] Statical quantum chemical methods indicated that the hydrogen bond is not the most important interaction for ion pairs with respect to the total interaction energy.[23] In contrast, different established analysis methods gave rise to hydrogen bonding in several ion pairs, thus the presence and importance of hydrogen bonds in ILs are undoubtedly proven from theory[23,26,28–30] and experiment.[31–33] However, the question of how long a particular anion–cation co-conformer is populated in the liquid state has not been extensively studied as stated above.[28] In ref. 28 it was concluded that the term "hydrogen bond" should, for now, be treated with care to characterise the cation–anion contacts.

Besides hydrogen bonding and its duration times, already on the level of cation–anion association, *i.e.*, ion pairing, much controversy has appeared in the literature.[34–36] The major reason for this stems from the indirect nature of measurement of the extent of the ion pairing, which often relies on heavy assumptions, such as unity charges in the supporting equations. Previously, it was shown[35–40] that using unity charges for ILs is questionable, because substantial charge transfer takes place in ILs.[35,36,39,40] By slightly shifting from the salt-like to a molecular liquid-like system *via* the decreased charges, the charge transfer also fluidizes the ionic liquid.[35,36]

The dynamics of ILs in terms of lifetimes has been studied previously.[16–18,20–22,41] In *ab initio* molecular dynamics (AIMD) simulations of $[C_2C_1Im][SCN]$ (HB donor–acceptor-hydrogen atom angle = 30°), the geometric picture indicated a superior role in terms of strength for the most acidic hydrogen bond (at H2, see Fig. 1 for labelling) as compared to the two other hydrogen atoms at the rear, in accordance with the literature.[17] However, the continuous (def. see next Section 2) hydrogen bond dynamics at H2 was observed to decay faster than the corresponding dynamics at the rear protons of the imidazolium ring (H4 and H5). Neglecting the directionality led to dynamics which reflect the geometrical analysis and which are in accordance to a non-linear hydrogen bond as discussed by Hunt and coworkers.[27,29] Two movements were identified, first, a fast (<0.3 ps) hopping of the anion above and below the imidazolium ring and second,

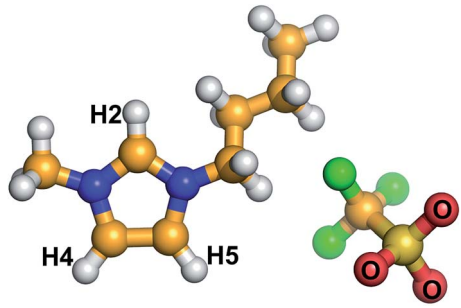


Fig. 1 Labelling as used in the article. Left: 1-Butyl-3-methylimidazolium cation and right: trifluoromethanesulfonate (triflate, [OTf]) anion (brown: carbon; blue: nitrogen; white: hydrogen; red: oxygen; yellow: sulfur; green: fluorine).

translational motion of the anion away from the cation in-plane of the imidazolium ring (5–10 ps).[17]

In a molecular dynamics (MD) simulation study of $[C_4C_1Im][PF_6]$ (HB angle = 30°), weak hydrogen bonds were found as indicated by their short lifetimes, which resulted from the fast rotational motion of anions.[18] As the magnitude of the activation energy related to the hydrogen bond relaxation time was observed to be close to the activation energy for anion reorientation, it was assumed that the rotation of the anion leads to the rapid breaking and forming/re-forming of hydrogen bonds.[18]

Comparing the hydrogen bond and the ion pair dynamics,[20] the shortest correlation time for the continuous hydrogen bond dynamics was again observed for the most acidic hydrogen atom (H2) in $[C_4C_1Im][Br]$ (studied at 360, 373, 402, 431, and 460 K and at a 30° angle criterion), closely followed by the continuous hydrogen bond dynamics of the rear hydrogen atoms (H4 and H5) in accordance with the literature.[16–18] The correlation time for the continuous ion pair dynamics (for an ion pair consisting only of one cation and its nearest anion) was only one order of magnitude larger. If instead ion cage dynamics based on distance criteria to include all neighbouring counter-ions were applied, the dynamics were found to be another order of magnitude larger.[20] Correlation times for the reorientation of the different cation parts were also considered and they were found to be larger than the correlation times of the continuous hydrogen bond dynamics and the correlation times of the continuous ion pair dynamics.[20] The largest correlation time for reorientation was calculated for the imidazolium ring. It was observed to be on the same timescale as the continuous cage dynamics.[20]

Using MD simulations, different charges on the cation and anion of the $[C_4C_1Im][Br]$ IL were studied.[21] Increasing the strength of the hydrogen bond led to a reduced mobility. Interestingly, the extreme situation of the anti-hydrogen bond (negative charge at the proton) also affected the properties at the other hydrogen atoms. Large effects of the altered charges were reflected in the ion pair dynamics. This is probably due to the fact that often the next neighbour determining the IP was the one at the most acidic proton for which the charge was altered. There were also large effects in the IC dynamics if the total charge or the hydrogen bond situation was changed. The cage and ion pair dynamics correlated well with the transport properties.[21]

Pensado *et al.* found while comparing for AIMD dispersion-corrected to uncorrected density functional theory,[41] that a given cation of [$C_2C_1$Im][SCN] (398.15 K, HB angle = 50°) preserves its environment for a longer time when dispersion is considered. The relaxation times of the dispersion-corrected trajectory were around twice those from the uncorrected trajectory. The effect of including dispersion corrections led also towards slower intermittent hydrogen-bond dynamics of the system. The HBs formed survived for a shorter time when dispersion was not taken into account, suggesting that important interactions between the anions and cations are omitted.[41]

HB dynamics have been investigated for [$C_2C_1$Im][Cl] (450.0 K) and [$C_4C_1$Im][Cl] (353.15 K) by Hunt and coworkers at HB angles of 30 and 60°.[22] The average HB number remained constant in a 100 K range, but the underlying dynamics of the HB changed dramatically.[22] The deformations of angles were found to be more relevant than bond stretching in determining the dynamics of individual HBs. A decay occurred on two timescales related to the magnitude of the deviation from linearity. For the intermittent HB, strong temperature dependent repeated breaking and reforming over a longer timescale was observed. In [$C_2C_1$Im][Cl] (450.0 K) hydrogen bonding with ring and alkyl chain hydrogen atoms occurred, ring reorientational dynamics were anisotropic and the corresponding dynamics were similar to the intermittent HB dynamics. In [$C_4C_1$Im][Cl] (353.15 K) ring hydrogen atoms dominated the hydrogen bonding and intermittent HB lasted for $\approx$5 ns, and ring reorientation occurred on a much slower timescale. The [$C_2C_1$Im][Cl] (450.0 K) favoured single HBs, but the individual ions often changed, while the [$C_4C_1$Im][Cl] (353.15 K) favoured bifurcated HBs with the same co-located ions.[22]

Very interesting model studies were carried out by Spohr and Patey.[42–44] They built up simple models in MD simulations. In the first study, the influence of ion size disparity was investigated.[42] The electrical conductivity first increased with size disparity, next it remained constant, then it decreased such that the conductivities of the 1 : 1 and 5 : 1 (cation : anion) systems were similar. This behaviour was explained by competing influences of both ion diffusion leading to an enhancement, and ion densities with the effect of reduction of conductivities at a constant packing fraction.[42] In the second model, the influence of charge location (cation charge moved away from its centre of mass) on the structure and transport properties was investigated.[43] As the charge was moved off centre, the electrical conductivity initially increased, and the shear viscosity decreased. However, after a certain threshold this behaviour was reversed. The formation of directional ion pairs that possess lifetimes (the correlation function decays in this case simply exponentially) strongly influenced the liquid properties.[43] The further the charge was moved off, the longer the directional ion pairs existed. These lifetimes ranged from 0.03 to 90 ps. The authors concluded that the directional ion pairing explains the anomalously low conductivities and high viscosities observed for some ILs.[43] A combination of both effects (size disparity and charge location) were investigated in a third study.[44] The upturn in viscosity with larger size disparity and charge dislocation was suggested to be mainly associated with directional ion pairs, and the formation of such pairs was mostly determined by charge dislocation. This observation was further supported by the fact that an increase in ion pair lifetimes coincided with the increase in viscosity for all models,[44] which is in turn in agreement with the correlation of ion cage and ion pair dynamics to transport properties in a realistic IL system.[21]

A pragmatic approach to harvest this correlation between ion pair dynamics and transport properties was recently suggested by Maginn and coworkers.[45] Based on previously established correlations between certain dynamics (ion pair and ion cage) in ILs and macroscopic properties,[21] they suggested to correlate the inverse of the ion pair dynamics in a single universal linear relationship to self-diffusivities and ideal ionic conductivities.[45] This relationship was independent of the type of IL and temperature. Considering the variety of ILs which were studied, their observation strongly suggested that the dynamics of ILs follow a universal mechanism governed by the formation and breaking of ion pairs and ion cages.[45]

Similarly, a computational study of the molecular origin of viscosity and subsequent correlation of the quantitative structure–property relationship approach and molecular dynamics simulations were carried out by Müller-Plathe and coworkers.[46]

HB dynamics of molecular liquids such as water (bulk and confined) has been extensively discussed in the literature.[47–59] For an excellent overview see ref. 52. In the pioneering work of Luzar and Chandler (ref. 51) it was demonstrated that the bond making and breaking are simple processes characterised by well-defined rate constants. What makes the HB dynamics apparently complicated is translational diffusion that introduces a continuum of timescales. They showed that these kinetics are understood in terms of the interplay between diffusion and HB dynamics. In their phenomenological model, translational diffusion determines whether a specific pair of water molecules are neighbours, and hydrogen bonds between such pairs form and persist at random with average lifetimes given by rate constants for bond breaking and reforming.[51]

Holm and coworkers were the first to determine reactive flux hydrogen bond lifetimes[16] for ILs (HB angle = 30°), and found them in the range of estimated values from the dielectric relaxation method. The following order of long lifetimes was observed: $[C_2C_1Im][Cl]$ (360 K) > $[C_2C_1Im][NTf_2]$ (288 K) > $[C_2C_1Im][BF_4]$ (257 K), which is due to the distribution of partial charges and the formation of networks in multi-atomic anion ILs.[16] Of course, the interactions of the anions and the imidazolium ring hydrogen atoms are stronger than those with the side chain hydrogen atoms.[16] The calculated hydrogen bond lifetimes were in the same order of magnitude as those of pure water and of some small primary alcohols.[16]

In this article, we evaluate the dynamics of one pure IL ($[C_4C_1Im][Br]$) applying a polarizable and standard (non-polarizable) force field. We investigate $[C_4C_1Im]$ [OTf] (3-butyl-1-methylimidazolium trifluoromethanesulfonate) at different temperatures and mixed with water. Difficulties when simulating water and ILs have been discussed by Maginn and coworkers.[60] Furthermore we consider the dynamics in the IL mixture $[C_4C_1Im][Cl]/[OTf]$. We reflect on the structure and then consider dynamics. In the final section we consider a possible correlation between intermittent as well as reactive flux IP dynamics and experimental viscosities. We end the article with some conclusions.

## 2 Theory of reactive flux dynamics and definitions

In the following, the methodology to describe hydrogen bond kinetics in liquid water introduced by Luzar and Chandler will be shortly summarised, for a full

description the reader is referred to the original articles.[50–52] The method relies on the definition of a hydrogen bond population operator $h(t)$, which equals unity if a particular tagged pair of (water) molecules is hydrogen bonded, and zero otherwise. As described below, in our selected ILs the cation is the hydrogen bond donor and the anion is the hydrogen bond acceptor for the pure ILs and for the IL mixtures. For the ILs mixed with water all three combinations, cation–anion, cation–water and water–anion, will be considered. Furthermore, we will also consider the population of ion pairs and ion cages as previously introduced by us.[20,21]

The time/ensemble average $\langle h \rangle$ (denoted by chevrons) of the population operator can be interpreted as the probability that a pair is hydrogen bonded. In an infinite or sufficiently large system, that probability will be zero and it is often neglected; in smaller systems, it won't, thus it shall be explicitly considered here. Using $h(t)$ or its fluctuation from equilibrium $\delta h(t) = h(t) - \langle h \rangle$, one can define a hydrogen bond time–correlation function

$$c(t) = \frac{\langle \delta h(t) \delta h(0) \rangle}{\langle \delta^2 h(0) \rangle} \approx \frac{\langle h(t) h(0) \rangle}{\langle h(0) \rangle}, \tag{1}$$

where the approximation holds if the system is sufficiently large, so that $\langle h \rangle \approx 0$, which implies $\delta h(t) \approx h(t)$. This function measures the fluctuations of hydrogen bond populations in time, independent of possible bond breaking events, *i.e.*, it is an intermittent time–correlation function, as introduced by Rapaport.[49] It can also be interpreted as the conditional probability that an initially hydrogen bonded pair is still or again bonded at a time $t$ later. Apart from these intermittent time–correlation functions, we will also consider the corresponding continuous functions for all dynamics (HB, IP and IC).[49] Contrary to the intermittent function the HB is broken once the donor and acceptor depart from each other even if only for a short time and even if they reform to HB afterwards.

According to Onsager's regression hypothesis, the same laws that govern the time evolution of the hydrogen bond time–correlation function, drive the decay of an initial non-equilibrium population $\overline{\delta h}(0)$ towards the equilibrium, with $\overline{\delta h}(t) = \overline{h}(t) - \langle h \rangle$. Thus

$$c(t) = \frac{\langle \delta h(t) \delta h(0) \rangle}{\langle \delta^2 h(0) \rangle} = \frac{\overline{\delta h}(t)}{\overline{\delta h}(0)}, \tag{2}$$

where the overlines denote a non-equilibrium average. The rate of relaxation to equilibrium is given by

$$k(t) = -\dot{c}(t) = \frac{\left\langle h(t) \dot{h}(0) \right\rangle}{\langle \delta h^2(0) \rangle} = -\frac{\left\langle [1 - h(t)] \dot{h}(0) \right\rangle}{\langle \delta h^2(0) \rangle}, \tag{3}$$

which follows from the definition of $c(t)$, by exploiting the time invariance of time–correlation functions, and because of the identity $\langle \dot{h}(0) \rangle = 0$. The quantity $-\dot{h}(0) = -(\mathrm{d}h/\mathrm{d}t)_{t=0}$ is the integrated flux departing the hydrogen bond configuration space at time zero. The function $k(t)$ measures the average of that flux for those trajectories, where the bond between a tagged pair of molecules is broken at a time $t$ later, hence its name: reactive flux hydrogen bond time–correlation function. Its zero time value is the transition state theory estimate of the rate of relaxation, $k_{\mathrm{TST}}$.[48] In the reactive flux formalism $k_{\mathrm{TST}}$ is corrected by a time dependent transmission coefficient.[61]

In bulk water, $k(t)$ reveals several motions leading to bond breaking.[50] A quick change on the timescale of 0.1 ps is primarily due to librations, followed by interoxygen vibrations on timescales of 0.1 to 0.2 ps. Beyond that transient period of ~0.3 ps, a continuum of timescales follows, resulting in a monotonic, non-exponential decay. Luzar and Chandler showed[51,52] that this behaviour can be understood with a simple diffusion picture: after bond-breaking, a pair can drift apart, and similarly, diffusion of two molecules towards each other can lead to bond-reforming. In order to investigate this, they separated the contributions to $k(t)$ according to whether a pair did or did not move apart after bond breaking, *i.e.*, by investigating the restrictive reactive flux time–correlation function

$$k_{\mathrm{in}}(t) = -\frac{\left\langle H(t)[1-h(t)]\dot{h}(0)\right\rangle}{\langle \delta h^2(0)\rangle}. \tag{4}$$

The vicinity operator $H(t)$ is responsible for that partitioning. It is unity if the particular tagged pair has not yet drifted apart, and zero otherwise. Thus, in the case of water it is usually defined as the oxygen atom–oxygen atom distance not further apart than the first minimum distance of the radial distribution function (RDF), thus 350 pm. The conditional probability that an initially bonded pair is broken, but has not drifted apart at a time $t$, is given by

$$n(t) = \int_0^t k_{\mathrm{in}}(\tau)\mathrm{d}\tau = \frac{\langle H(t)[1-\delta h(t)]\delta h(0)\rangle}{\langle \delta h^2(0)\rangle}. \tag{5}$$

The probabilities $c(t)$ and $n(t)$ correspond to local populations that can interconvert. A phenomenological description of their kinetics that is consistent with simulation data is

$$-\dot{c}(t) = k_{\mathrm{f}}c(t) - k_{\mathrm{b}}n(t), \tag{6}$$

where the forward and backward rate constants $k_{\mathrm{f}}$ and $k_{\mathrm{b}}$ are the rate constants of hydrogen bond breaking and forming. The physical meaning of $\tau_{\mathrm{hb}} = 1/k_{\mathrm{f}}$ is that of the average hydrogen bond lifetime.

For our three dynamics, hydrogen bond, ion pair, and ion cage, we define a population operator in analogy to Luzar's[51,52] hydrogen bond population operator $h(t)$ as described above for the hydrogen bond.

The events are populated:

• As a hydrogen bond, if the donor–acceptor-hydrogen atoms are arranged in an angle of less than 60 degrees (see also Fig. 3 as an example) and if the acceptor and the hydrogen atom are closer than the first minimum of the RDF. Furthermore, if we consider the reactive flux correlation function the centre of the ring of the imidazolium cation (c(R)), and the centre of mass of the anion (c(A)) should be closer than the distance of the first minimum in the RDF.

• As an ion pair, if the cation and anion are nearest neighbours with respect to the centre of the ring of the cation and the centre of mass of the anion distance. Furthermore, if we consider the reactive flux correlation function the c(R) and the c(A) should be closer than the distance of the first minimum in the RDF. Please note, this definition can be generally applied to the centre of mass/the ring.

Although the name is not correct with respect to physics we keep it in order to be able to compare to the literature.

• As an ion cage, if the central ion is surrounded by counter-ions in a radius smaller than the first minimum of the RDF between the c(R) and c(A). Thus, more than one neighbour is considered for the central ion.

# 3 Systems investigated

The extended description of the computational details can be found in the ESI.† We used the OPLS-AA force field,[62] which was extended by the parameter set for the imidazolium ring unit and the halides.[63] The applied parameters for the triflate anions were taken from ref. 64. The charges were scaled by a factor of 0.8 for all cations and anions. The water model is chosen to be the nonpolarizable SPC/E[65] for all calculations. Details of the polarizable force field deviate and are given in the ESI.†

In this study we consider the following IL systems:

• The $[C_4C_1Im][Br]$ liquid for comparing the non-polarizable (FF) and polarizable force field (pol-FF)[66,67] at 386 K.

• The temperature dependence at 293 K, 323 K, 353 K, 373 K, and 393 K of $[C_4C_1Im][OTf]$.

• The ionic liquid/molecular liquid mixture $[C_4C_1Im][OTf]$/water at four different mole fractions of the IL (0.39, 0.58, 0.66, and 0.82) taken from ref. 68 at 293 K.

• The ionic liquid mixture $[C_4C_1Im][Cl]$/[OTf] at $x = 0.000$, 0.192, 0.303, and 0.402 mole fractions of $[C_4C_1Im][Cl]$ at 298 K.

# 4 Results: structure

## 4.1 The effect of a polarizable force field on $[C_4C_1Im][Br]$

In Fig. 2 we present the radial distribution functions (RDF) for the ring hydrogen atoms with a simple anion like $[Br]^-$. The location of the first maximum and minimum together with the coordination number obtained from the corresponding number integrals (at the distance of the first minimum) can be found in Table 1. Obviously H2 forms stronger hydrogen bonds than H4/5, because it is more acidic,[23,26] which is reflected in the higher peaks and larger coordination number per hydrogen atom. This is in agreement with MD simulations and empirical refinement to model experimental data by Bowron *et al.*, where the authors also found a more pronounced coordination at H2.[69] Upon applying the polarizable force field larger distances are found, see also ref. 70. Furthermore, the coordination number decreases with the polarizable force field (see Table 1), but the relative behaviour remains the same. The ions are surrounded by approximately five counterions, also here the polarizable force field decreases the number slightly.

Unfortunately, the force field is unable to resolve distance differences at the ring protons, which are, for example, observed in AIMD simulations[17] and experiments.[71] Thus, the approach by Maginn to treat the ring protons on equal footing when applying FF for the MD seems reasonable.[45] In the present work, we distinguish front (H2) and rear (H4 and H5) hydrogen bonding (see Fig. 1).

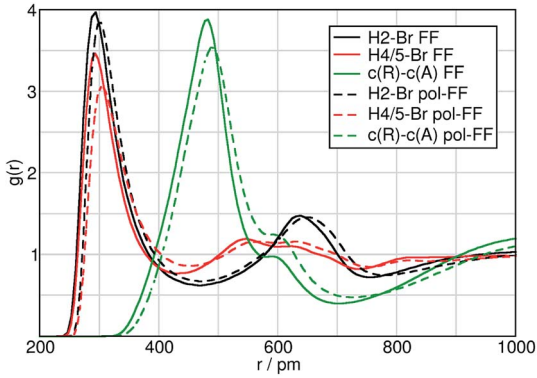


Fig. 2 Cation–anion radial distribution functions (RDFs). Black: H2; red: H4/5; green: RDFs between the centre of the ring of c(R) and the centre of mass of anion c(A). Solid line: standard force field; dashed line: polarizable force field. Please note, for clarity we show only a range of the RDF, the full functions can be found in the ESI,† these decay properly to 1.

### 4.2 Temperature dependency of the structure in $[C_4C_1Im][OTf]$

The temperature dependent RDFs are shown in the ESI,† and the corresponding distances of the first maximum $r$(max), first minimum $r$(min) as well as the coordination numbers from the number integrals are listed in Table 2.

Obviously, there is more variation in the peak heights than in the peak positions (see ESI†). Since the uncertainty of the distances is ~5 pm, resolving these subtle changes in positions within the present temperature range is not possible. However, a rough trend points to a bond elongation with temperature, indicating a weakening of the HB, in good agreement with the decrease in coordination numbers and peak heights. The exception is the very low temperature of 293 K, which is already close to the melting temperature of 290 K measured by Tokuda *et al.*,[34] and 286 K measured by Brennecke and coworkers.[72] Interestingly, the coordination number at 373 K and 393 K is much larger than that for the bromide at 386 K, which is probably due to the fact that three oxygen atoms are available for coordination instead of only one bromide ion. On average the cation is surrounded by 5.8–6$[OTf]^-$ anions, while it is surrounded by only approximately 5.3 $[Br]^-$ anions. Hardacre *et al.* obtained similar results (at 323 K by MD and neutron scattering) *via* integrating up to 750 pm from the ring centre, namely 5.3 for

Table 1 Distance of the first maximum $r$(max), first minimum $r$(min) (in pm) and number integral (NI) at $r$(min) from the reference to the observed particle in $[C_4C_1Im][Br]$ for H2 and H4/5 as well as for the centre of ring-$[Br]^-$ (c(R)–c(A)). $\overline{NI}$ is the number integral from the observed to the reference particle. If no number is given, NI = $\overline{NI}$. "FF": standard force field; "pol-FF": polarizable force field. $T$ = 386 K

| | $r$(max)/$r$(min)/NI/$\overline{NI}$ | | |
|---|---|---|---|
| | H2–Br | H4/5-Br | c(R)–c(A) |
| FF | 293/468/1.6 | 293/428/1.3/2.5 | 483/703/5.3 |
| pol-FF | 303/473/1.4 | 303/458/1.3/2.6 | 488/723/5.0 |

Table 2 $r$(max) (pm), $r$(min) (pm), NI and $\overline{\text{NI}}$ as in Table 1, in [$C_4C_1$Im][OTf] for H2–O, H4/5–O and c(R)–c(A) at different temperatures

| | $r$(max)/$r$(min)/NI/$\overline{\text{NI}}$ | | |
|---|---|---|---|
| $T$ | H2–O | H4/H5–O | c(R)–c(A) |
| 293 | 263/403/2.7/0.9 | 258/373/1.9/1.2 | 528/793/6.0 |
| 323 | 258/408/2.7/0.9 | 258/378/1.9/1.2 | 528/793/5.9 |
| 353 | 258/403/2.6/0.9 | 258/373/1.7/1.2 | 533/793/5.8 |
| 373 | 258/403/2.5/0.8 | 258/378/1.8/1.2 | 533/798/5.8 |
| 393 | 258/403/2.4/0.8 | 263/383/1.8/1.2 | 533/798/5.8 |

[$C_4C_1$Im][$PF_6$], 4.9 for [$C_6C_1$Im][$PF_6$], 4.4 for [$C_8C_1$Im][$PF_6$] or 6.8 for [$C_1C_1$Im][$PF_6$].[73] Furthermore, Bowron obtained (at 323 K from MD and neutron diffraction) 6.9 for [$C_2C_1$Im][OAc] by integrating up to 700 pm.[69]

In the combined distribution functions (CDFs), given in Fig. 3, the occurrences of different HB geometries are shown for two temperatures. It is apparent that for the IL the choice of a donor–acceptor-hydrogen angle of 60° is reasonable and the temperature dependency in the first (below 200 pm) but even more in the second peaks (~600 pm) is visible.

### 4.3 Mixtures of [$C_4C_1$Im][OTf] with water

The c(R)–c(A), c(A)–c(W) and the c(R)–c(W) (where c(R) is the geometrical center of the cationic ring, c(A) is the center of mass of the anion, and c(W) is the center of mass of the water molecule) RDFs are shown in Fig. 4 and colour-coded for different mole fractions. It is apparent that all three functions display a pre-

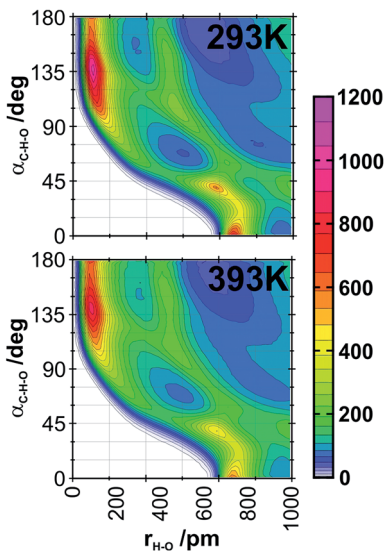


Fig. 3 CDFs for occurring HB geometries in [$C_4C_1$Im][OTf], HB angle ($\alpha_{C-H-O}$) *vs.* the HB distance ($r_{H-O}$).

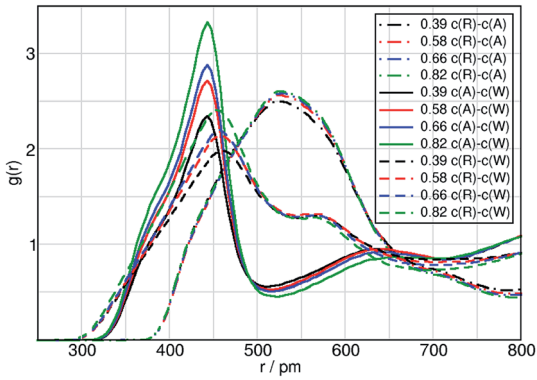


Fig. 4 RDFs of $[C_4C_1Im][OTf]$/water. Dashed-dotted: c(R)–c(A); solid: c(A)–c(W); dashed: c(R)–c(W). Black: $x = 0.39$ IL; red: $x = 0.58$ IL; blue: $x = 0.66$ IL; green: $x = 0.82$ IL. Please note, for clarity we show only a range, the full functions can be found in the ESI.† These decay properly to 1.

shoulder. Post-peaks are also observable for the c(R)–c(A) and the c(W)–c(A) function indicating a rather complex coordination pattern with multiple interaction sites.

Upon dilution, *i.e.*, going from green to black, all functions show a decrease in their first peak heights. In the case of the cation–anion interplay this means that the cation–anion coordination decreases from 5.8 to 5.3 (see Table 3). The number integrals for water–water (c(W)–c(W)) increase upon dilution. For the mixed IL–water interactions (c(R)–c(W) and c(A)–c(W)) we observe the same trends, see the NI values in Table 3, all coordination numbers increase when more water is added. The opposite trend is observed for the water–IL interaction, reflected in the $\overline{NI}$ values, which decrease slightly upon the dilution of the IL. In other words, by the addition of water to the system the number of water molecules around the IL ions increases, but the water molecules are interacting more extensively with each other than with the cation or the anion. This observation points to the change in the size of hydrogen bonding networks of water clusters and aggregates in the system upon dilution. According to the number integrals, the cations are surrounded by many more water molecules than the anions. The cations are indeed significantly larger than the anions, and therefore they could, in principle, be in contact with more water molecules at a time. However, based on the general wisdom in the literature of IL/water mixtures, the anions interact stronger with the water molecules than the cations, which—together with the altogether higher and sharper and higher peaks in the anion–water RDFs compared to those for the cation–water interplay—suggests that the differences in number integrals do not reflect on the trends in the strength of these interactions. In fact, since the anions are highly correlated with the cations, the very broad peak in the c(R)–c(W) RDFs necessarily includes those water molecules that are in hydrogen bonds with the anions, neighbouring the reference cation. Accordingly, the number integrals in Table 3 are not coordination numbers *per se*.

Beside the local structure arising from hydrogen bonding and other polar–polar interplay between the water and the IL and between the IL ions, the

Table 3 $r$(max) (pm), $r$(min) (pm), NI and $\overline{\text{NI}}$ as in Table 1, in [$C_4C_1$Im][OTf]/water for c(R), c(A) and c(W) for different mole fractions. Temperature = 293 K. $x_{IL}$ gives the mole fraction of the IL. Ring hydrogen functions are given in the ESI. The last block shows the domain count[14] and the number of molecules per domain/cluster

| | $r$(max)/$r$(min)/NI/$\overline{\text{NI}}$ | |
|---|---|---|
| $x_{IL}$ | c(R)–c(A) | c(W)–c(W) |
| 0.39 | 528/783/5.3 | 273/343/2.1 |
| 0.58 | 533/788/5.6 | 273/348/1.6 |
| 0.66 | 528/793/5.8 | 273/353/1.3 |
| 0.82 | 528/788/5.8 | 273/348/0.8 |

| | $r$(max)/$r$(min)/NI/$\overline{\text{NI}}$ | |
|---|---|---|
| $x_{IL}$ | c(R)–c(W) | c(A)–c(W) |
| 0.39 | 463/703/5.8/3.8 | 443/513/1.9/1.2 |
| 0.58 | 458/703/3.0/4.0 | 443/513/1.1/1.4 |
| 0.66 | 458/703/2.1/4.1 | 443/513/0.8/1.5 |
| 0.82 | 453/713/1.0/4.2 | 443/523/0.4/1.8 |

| | Domain count | | |
|---|---|---|---|
| $x_{IL}$ | Polar | Nonpolar | Water |
| 0.39 | 1.0 (197) | 5.9 (33) | 24.8 (12) |
| 0.58 | 1.0 (288) | 6.8 (42) | 53.0 (4) |
| 0.66 | 1.0 (330) | 6.8 (49) | 59.1 (3) |
| 0.82 | 1.0 (410) | 6.6 (62) | 52.8 (2) |

mesoscopic behaviour of the components within the liquid must also be analysed to discuss and understand the full structure of the IL–water mixtures, and the underlying dynamic processes. With our newly developed domain analysis tool[14] it is possible to analyse how the defined logical units (subsets) of the liquid are arranged in the system, that is, if they are systematically connected to one another to form larger clusters or domains. In this particular case we distinguished polar (anions, and the imidazolium ring with the $CH_2$ and $CH_3$ units connected to the nitrogen atoms), nonpolar (propyl group of the cation) and water as subsets. The corresponding data is presented in Table 3. Interestingly, the polar moieties stick together in all simulations, even in the most dilute systems. In contrast, but in agreement with previous simulations on pure ILs,[5,11] the nonpolar moieties do not form a continuous domain in the liquid, as the spatial extent of the present side chains is not sufficient for such behaviour. Instead, these alkyl groups apparently form smaller islands in the liquid, each of which gradually increase in size over the increase of the mole fraction of the IL in the solution. Finally, and perhaps most interestingly, the water molecules remarkably change their behaviour through the concentration range considered here. While in the case of the lowest mole fraction of the IL the water molecules form large clusters, consisting of on average 12 molecules, at the other extreme of the concentration range they are often present as single molecules in the

solution, and on average as dimers. This is in clear agreement with the number integral data, as discussed above.

### 4.4 Mixtures of $[C_4C_1Im][OTf]$ and $[C_4C_1Im][Cl]$

In Fig. 5 the chloride mole fraction dependent RDFs are given. Generally, the oxygen atoms coordinate with shorter distances to the ring hydrogen atoms of the cations than the chloride, simply due to the difference in radius between oxygen and chloride. Since the charge is highly delocalized in the triflate anion, the interaction with the individual oxygen atoms are generally weaker than with the chloride anion, represented by the remarkable differences in peak heights in Fig. 5.

Upon dilution of the $[C_4C_1Im][OTf]$ by the chloride, we observe a slight decrease in peak heights for both kinds of RDFs. For the O–H RDFs this finding is somewhat unexpected, since with the dilution of the [OTf] anions the peaks should naturally increase. Accordingly, these changes indicate that the stronger interacting chloride anions remove the [OTf] anions from the strongest hydrogen bond donor sites. Inspection of the coordination numbers in Table 4 shows that upon dilution the [OTf] anion generally decreases while the [Cl] anion coordination increases around the cation. Interestingly, the average number of [OTf] anions around the cation decreases significantly more than the increase in the number of [Cl] anions around the same species, in agreement with the aforementioned trends in the peak heights.

## 5 Results: dynamics

### 5.1 Pure $[C_4C_1Im][Br]$ and $[C_4C_1Im][OTf]$ systems

Since the peak positions in the RDFs have an uncertainty of $\pm 5$ pm, the distance criteria can be defined with a certain error for the dynamics results. In order to estimate the robustness of the dynamics, we calculated the changes in the results for $[C_4C_1Im][Br]$ with a 1 pm, 5 pm and 10 pm deviation from our standard distance criteria. For the hydrogen bond lifetime we found <0.25% deviation for

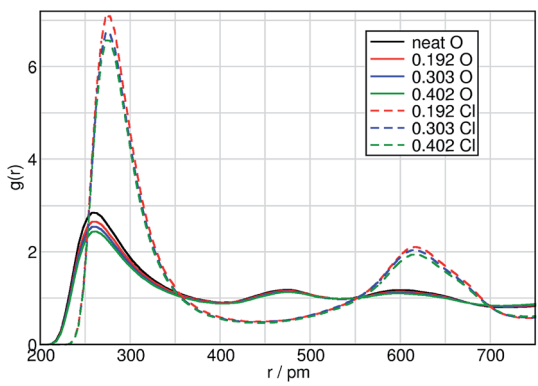


Fig. 5 Chloride mole fraction dependent H2–O/Cl RDFs of $[C_4C_1Im][OTf]/[Cl]$. Please note, for clarity we show only a range, the full functions can be found in the ESI.† These decay properly to 1.

Table 4 $r$(max) (pm), $r$(min) (pm), NI and $\overline{\text{NI}}$ as in Table 1, in $[C_4C_1Im][OTf]/[Cl]$ for H2–O/Cl and H4/H5–O/Cl centre of mass/ring functions. $x$ = mole fraction of $[C_4C_1Im][Cl]$

| | $r$(max)/$r$(min)/NI/$\overline{\text{NI}}$ | | |
|---|---|---|---|
| $x$ | H2–O | H2–Cl | H4/5–O |
| 0.000 | 258/403/2.7/0.9 | — | 258/373/1.8/1.2 |
| 0.192 | 263/403/2.2/0.9 | 278/438/0.3/1.5 | 258/373/1.4/1.2 |
| 0.303 | 258/403/1.9/0.9 | 273/438/0.5/1.5 | 258/373/1.2/1.2 |
| 0.402 | 263/403/1.6/0.9 | 273/438/0.6/1.5 | 258/373/1.0/1.2 |
| | $r$(max)/$r$(min)/NI/$\overline{\text{NI}}$ | | |
| $x$ | H4/5–Cl | c(R)–c(OTf) | c(R)–c(Cl) |
| 0.000 | — | 533/793/6.0/6.0 | — |
| 0.192 | 278/423/0.3/3.0 | 533/788/4.8/5.9 | 468/558/0.8/4.2 |
| 0.303 | 278/418/0.4/2.9 | 528/783/4.2/6.0 | 468/558/1.3/4.2 |
| 0.402 | 278/418/0.6/2.9 | 528/783/3.6/6.1 | 463/558/1.7/4.2 |

both the continuous and intermittent functions. For the cage dynamics the intermittent function changed by <1% for all cutoff distances, while the continuous altered by <6% for the 10 pm and only 3% for the 5 pm change in the criteria. Influences from the angular criteria (not investigated here) can be also expected.

In Table 5 we list the continuous and intermittent dynamics for the pure systems in order to compare to the previous simulation data.[17,20] As expected, with increasing temperature the dynamics become faster, which fits well with the observation of increasing bond distances and reduced coordination numbers discussed in subsection 4.2. The application of the polarizable force field accelerates the dynamics tremendously, even if the charge reduction should, in principle, compensate the slow dynamics in the standard force field, which it apparently does not. Generally, the IP and HB dynamics are of the same order of magnitude. However, the IP dynamics are slower than the HB dynamics, due to the lack of directionality; the only exceptions are observed in the case of the H4/5 HBs in the $[Br]^-$ system. The ion cage dynamics (considering all IPs within the

Table 5 Continuous and intermittent dynamics of $\tau^{H2}$: HB dynamics at H2; $\tau^{H4/5}$ at H4/5; $\tau^{IP}$ ion pair dynamics and $\tau^{IC}$ ion cage dynamics in ps. The HB data are obtained from the 200 ps long trajectory. All values in ps

| | Continuous/intermittent | | | |
|---|---|---|---|---|
| System | $\tau^{H2}$ | $\tau^{H4/5}$ | $\tau^{IP}$ | $\tau^{IC}$ |
| $[Br]^-$–FF | 0.7/188 | 1.1/172 | 0.9/221 | 74.2/942 |
| $[Br]^-$–pol-FF | 0.6/24 | 0.7/19 | 0.6/27 | 20.6/108 |
| $[OTf]^-$-293 | 0.9/1165 | 1.1/946 | 3.7/3069 | 169.9/14 969 |
| $[OTf]^-$-323 | 0.7/365 | 0.9/309 | 2.5/996 | 139.2/4569 |
| $[OTf]^-$-353 | 0.6/180 | 0.8/144 | 2.3/490 | 112.0/2222 |
| $[OTf]^-$-373 | 0.6/109 | 0.7/84 | 1.9/293 | 93.1/1295 |
| $[OTf]^-$-393 | 0.5/78 | 0.6/60 | 1.7/205 | 84.8/896 |

first minimum radius) are one order of magnitude slower than both IP and HB in accordance with previous observations.[17,20] The difference between IP and IC is less pronounced in the case of the pol-FF. The continuous dynamics are in all cases faster for H2 than for H4/5. This trend is, interestingly, the opposite for the intermittent dynamics. Considering that the difference between these two functions is the handling of the breaking and reforming of hydrogen bonds, this might indicate that the "strength" of the HB at H2 lies in its frequent reformation, which can make it, in that sense, longer living. This difference can clearly rise from the well-known facile switch between the "in-plane" and "on-top" positions of the anion at H2 (shown *e.g.* by the spatial distribution functions[74]), which allows the frequent cleavage and formation of the corresponding HB. The anions at the H4/5 position can, on the other hand, switch between these two ring hydrogen atoms at the rear. However, to do so, the anions have to occur in the space between the H4 and H5 atoms, which is, according to the spatial distribution of the anions around the cations in such ILs,[74] not the case. This, together with the continuous and intermittent dynamics data, allows us to conclude that the change between the "on-top" and "in-plane" orientation of the anion at H2 is more frequent than the H4–H5 change.

The reactive flux hydrogen bond data is exhibited in Table 6. The increase in the dynamics with applying the polarizable force field or increasing temperature is also apparent in the reactive flux data. In all cases the lifetimes of H2 are shorter than those of H4/5. Differences in the breaking and reforming of the HB are also visible when comparing the rates of the forward (breaking) and the backward (reformation) reaction. Comparing the reactive flux HB data with the IP results in Table 7, we observe also for these dynamics that IP is in general slower than the HB process. Again, the breaking and re-formation process are not the same, see

Table 6 Reactive flux HB lifetimes for the forward $\tau_f^{HB}$ (ps), the backward reaction $\tau_b^{HB}$ (ps), and the transition state theory estimate of the rate of relaxation, $k_{TST}$ ($ps^{-1}$). All data are obtained from the 10 ns trajectory

| System | $\tau_f^{H2}$ | $\tau_b^{H2}$ | $k_{TST}$ |
|---|---|---|---|
| $[Br]^-$–FF | 52 | 110 | 1.77 |
| $[Br]^-$–pol-FF | 14 | 25 | 2.05 |
| $[OTf]^-$-293 | 304 | 569 | 1.84 |
| $[OTf]^-$-323 | 107 | 204 | 1.89 |
| $[OTf]^-$-353 | 51 | 97 | 1.81 |
| $[OTf]^-$-373 | 27 | 51 | 2.01 |
| $[OTf]^-$-393 | 21 | 41 | 1.80 |
| System | $\tau_f^{H4/5}$ | $\tau_b^{H4/5}$ | $k_{TST}$ |
| $[Br]^-$–FF | 60 | 125 | 1.14 |
| $[Br]^-$–pol-FF | 23 | 51 | 1.73 |
| $[OTf]^-$-293 | 443 | 924 | 1.26 |
| $[OTf]^-$-323 | 179 | 408 | 1.34 |
| $[OTf]^-$-353 | 99 | 236 | 1.49 |
| $[OTf]^-$-373 | 60 | 146 | 1.60 |
| $[OTf]^-$-393 | 41 | 101 | 1.64 |

the forward and backward rates. However, here the differences are much more pronounced than for the HB process. However, the rate of relaxation, that is, $k_{TST}$ values, are in all cases similar.

For the ion pair dynamics we also show the correlation functions corresponding to the reactive flux dynamics in Fig. 6–8. In Fig. 6 the semi-log plot of the ion pair rate function $k(t)$ for $[C_4C_1Im][Br]$ exhibits the according decay. The rate function $k(t)$ and thus $c(t)$ do not decay mono-exponentially, otherwise the graph in Fig. 6 would be a straight line after the transient time (Fig. 6 inset). Thus, the dynamics cannot be represented by a simple decay process, and lifetimes cannot be determined simply by integration. At short times of $k(t)$ (0.35 and 0.5 ps in the inset of Fig. 6), motions leading to ion pair breaking are visible. The restricted rate function $k_{in}(t)$, from which by integration $n(t)$ is obtained, can be seen in Fig. 7.

In Fig. 8 we show the correlation plot relating the functions $c(t)$, $n(t)$ (see ESI†) and $k(t)$. At shorter times, the expected deviations occur. However, at larger values there are also deviations, which might originate from strong statistical uncertainties and which show that further simulations have to be carried out with varying simulation parameters in order to arrive at clearer behaviours of the unity plot.

In the following sections we will concentrate solely on the reactive flux data, since continuous as well as intermittent functions are in general problematic. The continuous HB correlation functions are ill-defined, because they strongly depend on the presumed location of the dividing surface. Thus HB lifetimes should not be extracted from continuous HB correlation functions, as their values heavily depend on the bond definition, as well as on the sampling frequency. While intermittent HB correlation functions are better defined in this respect, the caveat remains if these functions do not relax exponentially (which they do not in our cases, see ESI†), reflecting the fact that different dynamic processes contribute to the decay of these functions. Clearly, one should not determine intermittent HB lifetimes from the zero frequency part of the intermittent correlation function (*i.e.*, the integral of it) or by assuming a quasi-exponential decay of these functions. Such determinations are arbitrary as the results depend on a specific interval over which these functions were studied.

### 5.2 $[C_4C_1Im][OTf]$/water mixtures

The intermittent c(R)–c(A) IP lifetime at $x_{IL} = 0.39$ is 2048 ps, at 0.58 is 2037 ps, at 0.66 is 2552 ps, and at 0.82 is 2696 ps.

Table 7 Reactive flux IP lifetimes for the forward $\tau_f^{IP}$ (ps), the backward reaction $\tau_b^{IP}$ (ps), and the transition state theory estimate of the rate of relaxation, $k_{TST}$ ($ps^{-1}$). All data are obtained from the 10 ns trajectory

| System | $\tau_f^{IP}$ | $\tau_b^{IP}$ | $k_{TST}$ |
|---|---|---|---|
| $[Br]^-$–FF | 52 | 190 | 8.92 |
| $[OTf]^-$-293 | 611 | 2674 | 1.73 |
| $[OTf]^-$-323 | 240 | 1120 | 1.61 |
| $[OTf]^-$-353 | 126 | 568 | 1.60 |
| $[OTf]^-$-373 | 76 | 320 | 1.71 |
| $[OTf]^-$-393 | 65 | 228 | 1.65 |

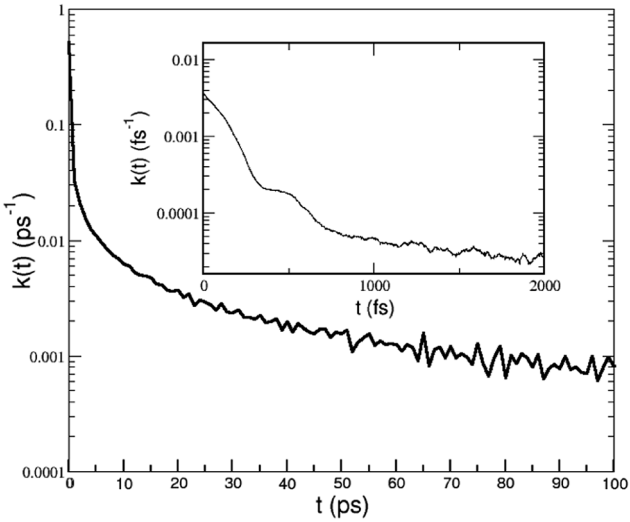


Fig. 6 Semi-log plot of the rate function $k(t)$ for the ion pair process in $[C_4C_1Im][Br]$. In the analysis the long trajectory was selected. The inset shows the analysis of the 200 ps trajectory, obviously at 0.35–0.5 ps a transient period is visible.

It is interesting to observe that the water–water interactions exhibit longer lifetimes in the IL-rich systems, which decrease gradually toward the more moist solutions. This is somewhat surprising, since with high $x_{IL}$ there is a higher number of available anions, which are not in interaction with other water molecules, suggesting that a cluster of water molecules would quickly break the connecting hydrogen bonds in order to interact with the stronger hydrogen bond acceptor anions instead. However, the smaller clusters of water (see Table 3)—often, in fact, a water dimer—in these liquids have apparently a very immobile hydrogen bond, sticking the molecules together for a longer time. With increasing water content, and therefore increasing size of water clusters, the

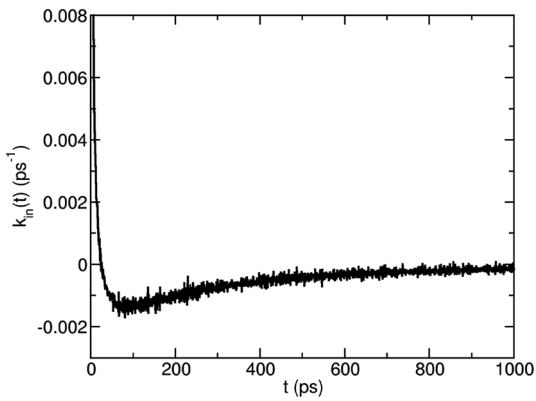


Fig. 7 The restricted rate function $k_{in}(t)$ for the ion pair process in $[C_4C_1Im][Br]$. In the analysis the long trajectory was selected.

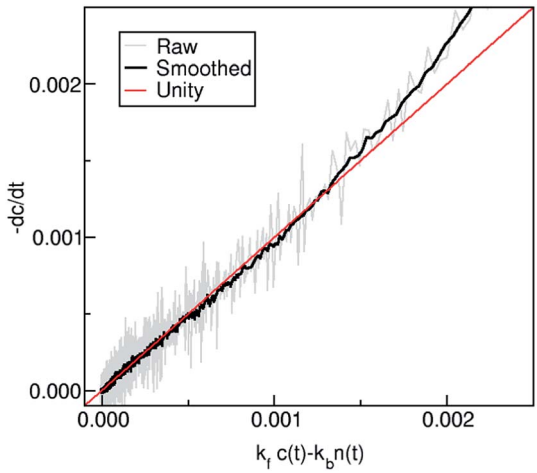


Fig. 8 Correlation plot for the ion pair process in $[C_4C_1Im][Br]$. Both axes are in $ps^{-1}$. In the analysis the long trajectory was selected. The fit to the line with unity slope was carried out from 160 to 8000 ps, and the values obtained for $k_f$ and $k_b$ are 0.019 $ps^{-1}$ and 0.005 $ps^{-1}$, see also Table 5.

individual water–water hydrogen bonds become significantly more mobile, which can be seen by the remarkable approximately four-fold increase in the lifetimes when the amount of water is reduced.

In almost all cases adding water (from $x = 0.82 \rightarrow 0.39$) leads to an acceleration of the ion pair (centre of mass/ring) dynamics, see Table 8. An exception is given by the backward reaction of the c(R)–c(W) interplay. At low mole fractions of water, the c(W)–c(A) dynamics are faster than all the others, while at high mole fractions the water–water dynamics are the fastest. All the dynamics involving water are faster than the cation–anion function.

Considering the individual HB dynamics (Table 9), the lifetimes involving ions are shorter compared to those from the centre of masses. It is important to point out here that the IL anion has multiple oxygen atoms as hydrogen bond acceptors, and accordingly, while the centre of mass–centre of mass distance does not change notably, the individual hydrogen bonds can flip from one acceptor site to the other. Again, faster dynamics toward the more moist systems can be observed (Table 9). Clear trends can be found for all forward lifetimes. In 2010, Feng and Voth presented diffusion coefficients of anions and water molecules in water mixtures with $[C_8C_1Im][BF_4]$ and $[C_8C_1Im][Cl]$. They found an overall trend of an exponentially increasing diffusion as a function of water mole fraction.[75] Recently, Sharma and Ghorai discussed why addition of water decreases the reorientational times for ions and increases their diffusion coefficients.[76]

### 5.3 Mixtures of $[C_4C_1Im][OTf]$ and $[C_4C_1Im][Cl]$

The results from the reactive flux dynamics for the IL mixtures are shown in Tables 10 and 11. Again, the backward process (reformation) is much slower in all cases than the forward process (dissociation). Considering the differences between the melting points of these two materials, could suggest that the addition

Table 8 Reactive flux ion pair interplay in the $[C_4C_1Im][OTf]$/water mixtures. $x_{IL}$ gives the mole fraction of the IL. 1st block: forward reaction (ps), 2nd block: backward reaction (ps); 3rd block: transition state theory (TST) approximation to the rate, thus a lower bound to the average IP lifetime ($ps^{-1}$)

| Forward | | | | |
|---|---|---|---|---|
| $x_{IL}$ | $\tau_f^{c(R)-c(A)}$ | $\tau_f^{c(R)-c(W)}$ | $\tau_f^{c(W)-c(A)}$ | $\tau_f^{c(W)-c(W)}$ |
| 0.39 | 399 | 270 | 287 | 146 |
| 0.58 | 454 | 351 | 328 | 232 |
| 0.66 | 487 | 454 | 387 | 238 |
| 0.82 | 500 | 459 | 407 | 663 |
| **Backward** | | | | |
| $x_{IL}$ | $\tau_b^{c(R)-c(A)}$ | $\tau_b^{c(R)-c(W)}$ | $\tau_b^{c(W)-c(A)}$ | $\tau_b^{c(W)-c(W)}$ |
| 0.39 | 1546 | 1201 | 576 | 156 |
| 0.58 | 1948 | 920 | 731 | 184 |
| 0.66 | 2064 | 892 | 933 | 147 |
| 0.82 | 2128 | 420 | 1013 | 467 |
| **TST** | | | | |
| $x_{IL}$ | $k_{TST}^{c(R)-c(A)}$ | $k_{TST}^{c(R)-c(W)}$ | $k_{TST}^{c(W)-c(A)}$ | $k_{TST}^{c(W)-c(W)}$ |
| 0.39 | 1.56 | 2.57 | 1.14 | 22.20 |
| 0.58 | 1.56 | 1.70 | 1.69 | 14.12 |
| 0.66 | 1.64 | 1.28 | 1.86 | 10.61 |
| 0.82 | 1.62 | 0.68 | 1.95 | 3.37 |

of the chloride salt might decrease the dynamics, and increase the lifetimes. In agreement, all the dynamics involving the [Cl] anion are slower than the analogous rearrangements with the [OTf] anion. This is in qualitative accordance with the shape of the RDFs shown in Fig. 5: the peaks related to the chloride-related interactions are sharper and higher, followed by a lower first minimum, indicating a certain barrier for the dislocation of the anion from the cation, while for the [OTf] anion the peaks are broader and the minima are shallower, indicating a facile movement.

Surprisingly, a slight decrease in the lifetime data is observed upon the addition of small amounts of $[C_4C_1Im][Cl]$ to $[C_4C_1Im][OTf]$, in agreement with the calculated viscosity values (see ESI†). The addition of further chloride species to the solution, however, decreases the dynamics, as the hydrogen bond and ion pair lifetimes continuously increase. Albeit interesting, the lifetimes showing a minimum at lower chloride concentrations is in clear contrast with the corresponding experimental viscosity values, which exhibit a continuous increasing trend throughout the whole concentration range. Thus, at this point, the detailed discussion of the dynamics of these mixtures is premature, and further comprehensive studies will be required for their full understanding.

Table 9 Hydrogen bond dynamics in the $[C_4C_1Im][OTf]$/water mixtures. $x$ gives the mole fraction of the IL

| Forward (ps) | | | |
|---|---|---|---|
| $x_{IL}$ | $\tau^{H2-O(A)}$ | $\tau^{H2-O(W)}$ | $\tau^{H4/5-O(A)}$ |
| 0.39 | 183 | 174 | 271 |
| 0.58 | 203 | 201 | 311 |
| 0.66 | 224 | 186 | 349 |
| 0.82 | 248 | 211 | 371 |
| $x_{IL}$ | $\tau^{H4/5-O(W)}$ | $\tau^{H(W)-O(A)}$ | $\tau^{H(W)-O(W)}$ |
| 0.39 | 149 | 119 | 175 |
| 0.58 | 176 | 127 | 228 |
| 0.66 | 193 | 150 | 264 |
| 0.82 | 217 | 181 | 258 |
| Backward (ps) | | | |
| $x_{IL}$ | $\tau^{H2-O(A)}$ | $\tau^{H2-O(W)}$ | $\tau^{H4/5-O(A)}$ |
| 0.39 | 372 | 395 | 648 |
| 0.58 | 399 | 439 | 677 |
| 0.66 | 439 | 374 | 772 |
| 0.82 | 488 | 452 | 809 |
| $x_{IL}$ | $\tau^{H4/5-O(W)}$ | $\tau^{H(W)-O(A)}$ | $\tau^{H(W)-O(W)}$ |
| 0.39 | 348 | 198 | 604 |
| 0.58 | 403 | 196 | 771 |
| 0.66 | 448 | 231 | 915 |
| 0.82 | 546 | 288 | 896 |
| TST ($ps^{-1}$) | | | |
| $x_{IL}$ | $k_{TST}^{H2-O(A)}$ | $k_{TST}^{H2-O(W)}$ | $k_{TST}^{H4/5-O(A)}$ |
| 0.39 | 1.87 | 2.55 | 1.40 |
| 0.58 | 1.70 | 1.84 | 1.37 |
| 0.66 | 1.88 | 2.13 | 1.49 |
| 0.82 | 1.85 | 2.15 | 1.34 |
| $x_{IL}$ | $k_{TST}^{H4/5-O(W)}$ | $k_{TST}^{H(W)-O(A)}$ | $k_{TST}^{H(W)-O(W)}$ |
| 0.39 | 1.79 | 2.20 | 0.87 |
| 0.58 | 1.60 | 1.27 | 3.24 |
| 0.66 | 1.94 | 2.16 | 1.65 |
| 0.82 | 1.98 | 2.33 | 6.12 |

# 6 Results: correlation of the viscosity and diffusivity with the ion pair dynamics

Correlations between lifetimes and diffusivity as well as between the latter and viscosities have been established.[21] Furthermore, a linear relationship between

Table 10 Lifetimes in $[C_4C_1Im][Cl]/[OTf]$ at 298 K. Please note, we do not distinguish the anion type. $x$ = mole fraction of $[C_4C_1Im][Cl]$

| Forward (ps) | | | | |
|---|---|---|---|---|
| $x$ | $\tau^{H2-O}$ | $\tau^{H2-Cl}$ | $\tau^{H4/5-O}$ | $\tau^{H4/5-Cl}$ |
| 0.000 | 242 | — | 385 | — |
| 0.192 | 210 | 514 | 258 | 592 |
| 0.303 | 328 | 858 | 394 | 853 |
| 0.402 | 428 | 999 | 461 | 1036 |
| **Backward (ps)** | | | | |
| $x$ | $\tau^{H2-O}$ | $\tau^{H2-Cl}$ | $\tau^{H4/5-O}$ | $\tau^{H4/5-Cl}$ |
| 0.000 | 461 | — | 847 | — |
| 0.192 | 413 | 706 | 216 | 974 |
| 0.303 | 647 | 1323 | 334 | 1267 |
| 0.402 | 882 | 1406 | 398 | 1532 |
| **TST ($ps^{-1}$)** | | | | |
| $x$ | $k_{TST}^{H2-O}$ | $k_{TST}^{H2-Cl}$ | $k_{TST}^{H4/5-O}$ | $k_{TST}^{H4/5-Cl}$ |
| 0.000 | 1.86 | — | 1.32 | — |
| 0.192 | 1.96 | 2.17 | 1.45 | 0.99 |
| 0.303 | 2.05 | 2.40 | 1.35 | 1.14 |
| 0.402 | 2.37 | 2.24 | 1.57 | 1.06 |

the calculated self-diffusivities and the inverse of IP or IC lifetimes was observed by Maginn and coworkers.[45] A similar inverse linear relationship was also found for ideal ionic conductivity and these relationships were found to be independent of temperature and the nature of the IL.[45] Maginn and coworkers conclude that these observations connect macroscopic dynamic properties with local atomic-level motions and strongly suggest that the dynamics of ILs are governed by a universal ion pair or ion cage forming and breaking mechanism. Thus, in order to design an ionic liquid with enhanced dynamics, one should consider how to minimise IP lifetimes.[45]

Another way to change macroscopic dynamics is to mix the IL with impurities such as water or investigate IL mixtures. For this reason, we correlate the viscosity with the IP dynamics of all our investigated systems.

Table 11 Lifetimes in $[C_4C_1Im][Cl]/[OTf]$ at 298 K. Please note, we do not distinguish the anion type. $x$ = mole fraction of $[C_4C_1Im][Cl]$. $\tau$ values in ps and $k_{TST}$ in $ps^{-1}$

| | Int | Reactive flux | | |
|---|---|---|---|---|
| $x$ | $\tau^{IP}$ | $\tau_f^{IP}$ | $\tau_b^{IP}$ | $k_{TST}$ |
| 0.000 | 2289 | 506 | 2252 | 1.51 |
| 0.192 | 2148 | 447 | 1731 | 2.14 |
| 0.303 | 3716 | 698 | 2625 | 2.79 |
| 0.402 | 4912 | 816 | 2920 | 3.21 |

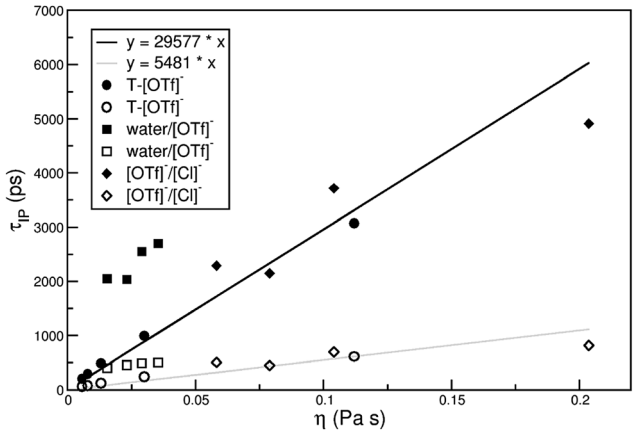


Fig. 9 Correlating calculated $\tau^{IP}$ (ps) with experimental viscosities (Pa s). Zero intercept is enforced in this fit. Correlation coefficients are 0.859 and 0.821 for the intermittent (solid symbols) and the reactive flux (open symbols) lifetimes, respectively.

All viscosity values are listed in the ESI.†[34,77–83] The temperature dependent values for $[C_4C_1Im][OTf]$ were taken from the group contribution model of Gardas *et al.*[84] for 373 K and 393 K.

Fig. 9 shows the correlation between the ion pair dynamics (intermittent and reactive flux) as well as the viscosities. There are thirteen points for each curve, 4 pertain to different mole fractions (diamonds), 5 to different temperatures (circles), and 4 to the mixtures with water (squares). The correlation is satisfying between the ion pair dynamics and the viscosity including not only temperature dependency, but also the mixture with chloride. Obviously, the water mixtures deviate mostly from the fitted curves. In this respect it will be interesting to

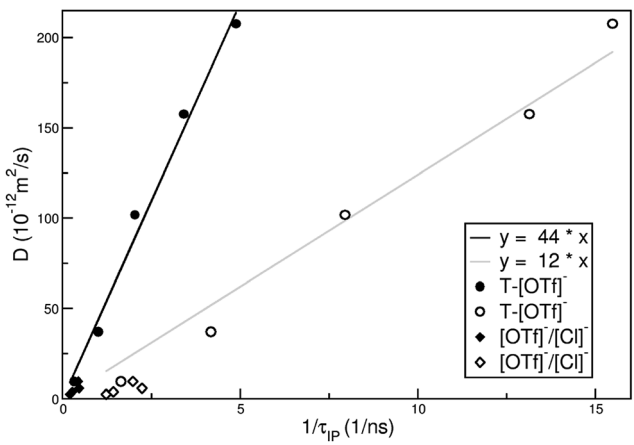


Fig. 10 Correlating calculated inverse $\tau^{IP}$ (ps) with experimental diffusivities ($10^{-12}$ $m^2$ $s^{-1}$). Zero intercept is enforced in this fit. Correlation coefficients are 0.995 and 0.997 for the intermittent (solid symbols) and the reactive flux (open symbols) lifetimes, respectively.

further investigate the reactive flux dynamics to reveal the detailed dynamics of IL systems.

Similarly we correlated the diffusivities to the inverse lifetimes in Fig. 10. The diffusivities have been measured by two of the authors (Clark and Welton) for the temperature dependent $[C_4C_1Im][OTf]$ liquid and the $[C_4C_1Im][Cl]/[OTf]$ mixture at 298 K, see ESI.† In order to obtain one number we followed the approach of Maginn and coworkers,[45] in which the average self-diffusivity was obtained by taking the average of the self-diffusivity of the cations and anion in a system, $D = (D_+ + D_-)/2$, where $D_+$ and $D_-$ were measured as the diffusion coefficient of the H atoms on the methyl groups and fluorine diffusion coefficients respectively. Due to the lack of experimental data for the mixtures with water we correlated only nine points. As stated above, this leads to an improvement of the correlation.

# 7 Conclusions

In order to obtain a broad picture of the structure and dynamics, we simulated several ionic liquid systems with the aid of flexible, atomistic, classical molecular dynamics simulations. In particular we studied the $[C_4C_1Im][Br]$ liquid with a non-polarizable and polarizable force field[66,67] at 386 K. The following systems were set up with a non-polarizable force field, namely a temperature dependent investigation at 293 K, 323 K, 353 K, 373 K, and 393 K of $[C_4C_1Im][OTf]$. This was supplemented by the ionic liquid/molecular liquid mixture of $[C_4C_1Im][OTf]$/water at four different mole fractions of the IL (0.39, 0.58, 0.66 and 0.82) taken from ref. 68 at 293 K. To complete the picture, simulations of ionic liquid mixtures $[C_4C_1Im][Cl]/[OTf]$ at $x = 0.000$, 0.192, 0.303, 0.402 mole fractions of $[C_4C_1Im][Cl]$ at 298 K were added.[78]

For the structure we observed the typical effects of a polarizable force field, like larger distances compared to the non-polarizable force field in accordance with previous studies.[70] Also smaller coordination numbers were observed for the polarizable variant. The temperature dependent calculation revealed that with increasing $T$ the distances are slightly longer. The cation is approximately surrounded by 5–6 anions which also only slightly changes to smaller numbers within the temperature range investigated here. The combined distribution functions clearly indicate that a 60 degree angle is the right choice for defining the hydrogen bond together with the first minimum in the according radial distribution function. In the moist IL system, adding water goes along together with a decrease in cation–anion coordination, the water–water coordination increases and so behave the IL–water number integrals. The coordination of the ions around the water decreases with added water in the IL. Our domain analysis tool reveals[14,85] that in all mole fractions the polar parts of the ions form one connected domain. The nonpolar parts of the IL ions become dispersed when water is added, and the water clusters/molecules grow in size. In the mixture with the chloride the coordination number changes between the two anions, but the number integral of the cation around the anions remains constant, about six around the trifluoromethanesulfonate anion and about four around the chloride anion.

For the dynamics, we analysed the continuous and intermittent functions in order to compare to the literature, but we mainly focused on the reactive flux dynamics, because they can give information about transient relaxation, showing

when most of the dynamics in a system is over. It automatically gives the transition state theory approximation to the rate, a lower bound to the average HB lifetime, that other methods extract from lengthy calculations, *e.g.* continuum HB correlation functions. The calculated rate function, combined with appropriate phenomenology, gives the actual HB lifetime (and even more, rate constants for both processes, breaking and reforming), which are all independent of the arbitrary HB definition in a simulation.

As expected, temperature accelerates the dynamics of all kinds of associations (HB and ion pair as well as ion cage). The polarizable treatment of the interactions also accelerates the dynamics and this occurs to such an extent that the charge reduction does not compensate this behaviour. By observing opposite trends in the continuous as well as the intermittent dynamics comparing the ring protons of the imidazolium cation, one can infer that the acidic H2 position provides more frequent breaking and reforming HB than the rear protons. In almost all cases adding water leads to an acceleration of the ion pair/centre of mass/ring dynamics. Finally, mixing the IL with the chloride anion leads to a tremendous decrease of the ion pair dynamics, as also reflected in the experimental viscosities. Thus, correlating the ion pair dynamics with the viscosities provides a simple tool to estimate whether new ILs or IL mixtures will have a decreased viscosity.

## Appendix

The computational details as well as a list of all methods and software packages used in this work can be found in the ESI.†[34,62–67,77–99]

## Acknowledgements

AL acknowledges the support from the Department of Energy, Basic Energy Sciences (DE-SC 0004406) and the National Science Foundation (CHE-1213814). SG was supported by the International Max Planck Research School for Reactive Structure Analysis for Chemical Reactions. We thank the Deutsche Forschungsgemeinschaft for support in the SPP 1708 under the project KI 768/15-1. MB acknowledges financial support by the Deutsche Forschungsgemeinschaft through project Br 5494/1-1.

## References

1 T. Welton, *Chem. Rev.*, 1999, **99**, 2071–2083.
2 B. Kirchner, *Ionic Liquids*, Springer, Berlin Heidelberg, 2010, vol. 290, pp. 213–262.
3 E. I. Izgorodina, *Phys. Chem. Chem. Phys.*, 2011, **13**, 4189–4207.
4 H. K. Kashyap, C. S. Santos, H. V. R. Annapureddy, N. S. Murthy, C. J. Margulis and E. W. Castner Jr, *Faraday Discuss.*, 2012, **154**, 133–143.
5 B. Kirchner, O. Hollóczki, J. N. Canongia Lopes and A. A. H. Pádua, *WIREs Comp. Mol. Sci.*, 2014, 202–214.
6 E. I. Izgorodina, Z. L. Seeger, D. L. A. Scarborough and S. Y. S. Tan, *Chem. Rev.*, 2017, **117**, 6696–6754.
7 Z. Hu and C. J. Margulis, *Proc. Natl. Acad. Sci. U. S. A.*, 2006, **103**, 831–836.
8 O. Russina and A. Triolo, *Faraday Discuss.*, 2012, **154**, 97–109.

 

9 S. M. Urahata and M. C. C. Ribeiro, *J. Chem. Phys.*, 2004, **120**, 1855–1863.
10 Y. T. Wang and G. A. Voth, *J. Am. Chem. Soc.*, 2005, **127**, 12192–12193.
11 J. N. Canongia Lopes and A. A. H. Pádua, *J. Phys. Chem. B*, 2006, **110**, 3330–3335.
12 H. Weber, O. Hollóczki, A. S. Pensado and B. Kirchner, *J. Chem. Phys.*, 2013, **139**, 084502.
13 K. Shimizu, C. E. S. Bernardes and J. N. Canongia Lopes, *J. Phys. Chem. B*, 2014, **118**, 567–576.
14 M. Brehm, H. Weber, M. Thomas, O. Hollóczki and B. Kirchner, *ChemPhysChem*, 2015, **16**, 3271–3277.
15 O. Hollóczki, M. Macchiagodena, H. Weber, M. Thomas, M. Brehm, A. Stark, O. Russina, A. Triolo and B. Kirchner, *ChemPhysChem*, 2015, **16**, 3325–3333.
16 B. Qiao, C. Krekeler, R. Berger, L. Delle Site and C. Holm, *J. Phys. Chem. B*, 2008, **112**, 1743–1751.
17 J. Thar, M. Brehm, A. P. Seitsonen and B. Kirchner, *J. Phys. Chem. B*, 2009, **113**, 15129–15132.
18 W. Zhao, F. Leroy, B. Heggen, S. Zahn, B. Kirchner, S. Balasubramanian and F. Müller-Plathe, *J. Am. Chem. Soc.*, 2009, **131**, 15825–15833.
19 B. S. Mallik and J. I. Siepmann, *J. Phys. Chem. B*, 2010, **114**, 12577–12584.
20 M. Kohagen, M. Brehm, J. Thar, W. Zhao, F. Müller-Plathe and B. Kirchner, *J. Phys. Chem. B*, 2011, **115**, 693–702.
21 M. Kohagen, M. Brehm, Y. Lingscheid, R. Giernoth, J. Sangoro, F. Kremer, S. Naumov, C. Iacob, J. Kärger, R. Valiullin and B. Kirchner, *J. Phys. Chem. B*, 2011, **115**, 15280–15288.
22 I. Skarmoutsos, T. Welton and P. A. Hunt, *Phys. Chem. Chem. Phys.*, 2014, **16**, 3675–3685.
23 S. B. C. Lehmann, M. Roatsch, M. Schoppke and B. Kirchner, *Phys. Chem. Chem. Phys.*, 2010, **12**, 7473–7486.
24 T. Steiner and G. R. Desiraju, *Chem. Commun.*, 1998, 891–892.
25 T. Steiner and G. R. Desiraju, *The weak hydrogen bond*, Oxford University Press, 1999.
26 P. A. Hunt, B. Kirchner and T. Welton, *Chem.–Eur. J.*, 2006, **12**, 6762–6775.
27 P. A. Hunt, C. R. Ashworth and R. P. Matthews, *Chem. Soc. Rev.*, 2015, **44**, 1257–1288.
28 V. Kempter and B. Kirchner, *J. Mol. Struct.*, 2010, **972**, 22–34.
29 I. Skarmoutsos, D. Dellis, R. P. Matthews, T. Welton and P. A. Hunt, *J. Phys. Chem. B*, 2012, **116**, 4921–4933.
30 S. Zahn, F. Uhlig, J. Thar, C. Spickermann and B. Kirchner, *Angew. Chem., Int. Ed.*, 2008, **47**, 3639–3641.
31 K. Fumino, A. Wulf and R. Ludwig, *Angew. Chem., Int. Ed.*, 2008, **47**, 3830–3834.
32 R. Cooper, A. M. Zolot, J. A. Boatz, D. P. Sporleder and J. A. Stearns, *J. Phys. Chem. A*, 2013, **117**, 12419–12428.
33 K. Fumino, A.-M. Bonsa, B. Golub, D. Paschek and R. Ludwig, *ChemPhysChem*, 2015, **16**, 299–304.
34 H. Tokuda, S. Tsuzuki, M. A. B. H. Susan, K. Hayamizu and M. Watanabe, *J. Phys. Chem. B*, 2006, **110**(39), 19593–19600.
35 O. Hollóczki, F. Malberg, T. Welton and B. Kirchner, *Phys. Chem. Chem. Phys.*, 2014, **16**, 16880–16890.

36 B. Kirchner, F. Malberg, D. S. Firaha and O. Hollóczki, *J. Phys.: Condens. Matter*, 2015, **27**, 463002.
37 F. Müller-Plathe and W. F. van Gunsteren, *J. Phys. Chem.*, 1995, **103**, 4756.
38 B. L. Bhargava and S. Balasubramanian, *J. Chem. Phys.*, 2005, **123**, 144505.
39 S. Kossmann, J. Thar, B. Kirchner, P. A. Hunt and T. Welton, *J. Chem. Phys.*, 2006, **124**, 174506.
40 T. G. A. Youngs and C. Hardacre, *ChemPhysChem*, 2008, **9**, 1548–1558.
41 A. S. Pensado, M. Brehm, J. Thar, A. P. Seitsonen and B. Kirchner, *ChemPhysChem*, 2012, **13**, 1845–1853.
42 H. V. Spohr and G. N. Patey, *J. Chem. Phys.*, 2008, **129**, 064517.
43 H. V. Spohr and G. N. Patey, *J. Chem. Phys.*, 2009, **130**, 104506.
44 H. V. Spohr and G. N. Patey, *J. Chem. Phys.*, 2010, **132**, 154504.
45 Y. Zhang and E. J. Maginn, *J. Phys. Chem. Lett.*, 2015, **6**, 700–705.
46 S. N. Butler and F. Müller-Plathe, *ChemPhysChem*, 2012, **13**, 1791–1801.
47 F. H. Stillinger, Theory And Molecular Models For Water, *Advances in Chemical Physics*, Wiley, Bell Laboratories, Murray Hill, New Jersey, vol. 31, 1975.
48 D. Chandler, *J. Chem. Phys.*, 1978, **68**, 2959.
49 D. C. Rapaport, *Mol. Phys.*, 1983, **50**, 1151–1162.
50 A. Luzar and D. Chandler, *Phys. Rev. Lett.*, 1996, **76**, 928–931.
51 A. Luzar and D. Chandler, *Nature*, 1996, **379**, 55–57.
52 A. Luzar, *J. Chem. Phys.*, 2000, **113**, 10663–10675.
53 A. Luzar, *Faraday Discuss.*, 1996, **103**, 29–40.
54 S. Bandyopadhyay, S. Chakraborty and B. Bagchi, *J. Am. Chem. Soc.*, 2005, **127**, 16660–16667.
55 J. Chanda and S. Bandyopadhyay, *J. Phys. Chem. B*, 2006, **110**, 23443–23449.
56 L. Hua, X. Huang, R. Zhou and B. J. Berne, *J. Phys. Chem. B*, 2006, **110**, 3704–3711.
57 R. Rousseau, E. Schreiner, A. Kohlmeyer and D. Marx, *Biophys. J.*, 2004, **86**, 1393–1407.
58 E. Schreiner, C. Nicolini, B. Ludolph, R. Ravindra, N. Otte, A. Kohlmeyer, R. Rousseau, R. Winter and D. Marx, *Phys. Rev. Lett.*, 2004, **92**, 148101.
59 H. Xu and B. Berne, *J. Phys. Chem. B*, 2001, **105**, 11929–11932.
60 E. Marin-Rimoldi, J. K. Shah and E. J. Maginn, *Fluid Phase Equilib.*, 2016, **407**, 117–125.
61 P. Hänggi, P. Talkner and M. Borkovec, *Rev. Mod. Phys.*, 1990, **62**, 251.
62 W. L. Jorgensen, D. S. Maxwell and J. Tirado-Rives, *J. Am. Chem. Soc.*, 1996, **118**, 11225–11236.
63 J. N. Canongia Lopes and A. A. Pádua, *J. Phys. Chem. B*, 2006, **110**, 19586–19592.
64 J. N. Canongia Lopes and A. A. Pádua, *J. Phys. Chem. B*, 2004, **108**, 16893–16898.
65 H. Berendsen, J. Grigera and T. Straatsma, *J. Phys. Chem.*, 1987, **91**, 6269–6271.
66 A. Dequidt, J. Devémy and A. A. H. Pádua, *J. Chem. Inf. Model.*, 2016, **56**, 260–268.
67 C. E. S. Bernardes, K. Shimizu, J. N. C. Lopes, P. Marquetand, E. Heid, O. Steinhauser and C. Schroder, *Phys. Chem. Chem. Phys.*, 2016, **18**, 1665–1670.
68 G. García-Miaja, J. Troncoso and L. Romaní, *J. Chem. Thermodyn.*, 2009, **41**, 161–166.
69 D. T. Bowron, C. D'Agostino, L. F. Gladden, C. Hardacre, J. D. Holbrey, M. C. Lagunas, J. McGregor, M. D. Mantle, C. L. Mullan and T. G. A. Youngs, *J. Phys. Chem. B*, 2010, **114**, 7760–7768.

 

70 O. Borodin, *J. Phys. Chem. B*, 2009, **113**, 11463–11478.
71 A. Elaiwi, P. B. Hitchcock, K. R. Seddon, N. Srinivasen, Y. Tan, T. Welton and J. A. Zora, *J. Chem. Soc., Dalton Trans.*, 1995, 3467–3472.
72 C. P. Fredlake, J. M. Crosthwaite, D. G. Hert, S. N. V. K. Aki and J. F. Brennecke, *J. Chem. Eng. Data*, 2004, **49**, 954–964.
73 C. Hardacre, J. D. Holbrey, C. L. Mullan, T. G. A. Youngs and D. T. Bowron, *J. Chem. Phys.*, 2010, **133**, 074510.
74 D. S. Firaha, M. Thomas, O. Hollóczki, M. Korth and B. Kirchner, *J. Chem. Phys.*, 2016, **145**, 204502.
75 S. Feng and G. A. Voth, *Fluid Phase Equilib.*, 2010, **294**, 148–156.
76 A. Sharma and P. K. Ghorai, *J. Chem. Phys.*, 2016, **144**, 114505.
77 M.-L. Ge, R.-S. Zhao, Y.-F. Yi, Q. Zhang and L. S. Wang, *J. Chem. Eng. Data*, 2008, **53**(10), 2408–2411.
78 M. T. Clough, C. R. Crick, J. Gräsvik, P. A. Hunt, H. Niedermeyer, T. Welton and O. P. Whitaker, *Chem. Sci.*, 2015, **6**, 1101–1114.
79 M. Tsamba, S. Sarraute, M. Traikia and P. Husson, *J. Chem. Eng. Data*, 2014, **59**(6), 1747–1754.
80 J.-M. Andanson, X. Meng, M. Traikia and P. Husson, *J. Chem. Thermodyn.*, 2016, **94**, 169–176.
81 G. McHale, C. Hardacre, R. Ge, N. Doy, R. W. K. Allen, J. M. MacInnes, M. R. Brown and M. I. Newton, *Anal. Chem.*, 2008, **80**, 5806–5811.
82 M. Shamsipur, A. A. M. Beigi, M. Teymouri, S. M. Pourmortazavi and M. Irandoust, *J. Mol. Liq.*, 2010, **157**, 43–50.
83 M. L. S. Batista, L. I. N. Tome, C. M. S. S. Neves, J. R. B. Gomes and J. A. P. Coutinho, *J. Mol. Liq.*, 2014, **192**, 26–31.
84 R. L. Gardas and J. A. P. Coutinho, *AIChE J.*, 2009, **55**, 1274–1290.
85 M. Brehm and B. Kirchner, *J. Chem. Inf. Model.*, 2011, **51**, 2007–2023.
86 G. Lamoureux and B. Roux, *J. Phys. Chem. B*, 2006, **110**, 3308–3322.
87 H. A. Lorentz, *Ann. Phys. Chem.*, 1881, **248**, 127–136.
88 D. Berthelot, *Compt. Rendus*, 1898, **126**, 1703–1855.
89 R. W. Hockney and J. W. Eastwood, *Computer simulation using particles*, CRC Press, 1988.
90 A. Khintchine, *Math. Ann.*, 1934, **109**, 604–615.
91 N. Wiener, *Acta Mathematica*, 1930, **55**, 117–258.
92 S. Nosé, *Mol. Phys.*, 1984, **52**, 255–268.
93 S. Nosé, *J. Chem. Phys.*, 1984, **81**, 511–519.
94 S. Plimpton, *J. Comput. Phys.*, 1995, **117**, 1–19.
95 L. Martínez, R. Andrade, E. G. Birgin and J. M. Martínez, *J. Comput. Chem.*, 2009, **30**, 2157–2164.
96 G. J. Martyna, M. L. Klein and M. Tuckerman, *J. Chem. Phys.*, 1992, **97**, 2635–2643.
97 R. L. Gardas, M. G. Freire, P. J. Carvalho, I. M. Marrucho, I. Fonseca, A. G. Ferreira and J. A. Coutinho, *J. Chem. Eng. Data*, 2007, **52**, 80–88.
98 T. Williams, C. Kelley, H. Bröker, J. Campbell, R. Cunningham, D. Denholm, E. Elber, R. Fearick, C. Grammes and L. Hart, http://www.gnuplot.info.
99 P. Turner, *XMGRACE, Version 5.1.19*, Center for Coastal and Land-Margin Research, Oregon Graduate Institute of Science and Technology, Beaverton, OR, 2005.